JYX
JYVÄSKYLÄN YLIOPISTO
UNIVERSITY OF JYVÄSKYLÄ

This is a self-archived version of an original article. This version may differ from the original in pagination and typographic details.

Author(s): Hiltunen, Vesa-Matti; Koskinen, Pekka Johannes; Mentel, Kamila K.; Manninen, Jyrki; Myllyperkiö, Pasi; Johansson, Andreas; Pettersson, Mika

Title: Making Graphene Luminescent by Direct Laser Writing

Year: 2020

Version: Accepted version (Final draft)

Copyright: © 2020 American Chemical Society

Rights: In Copyright

Rights url: http://rightsstatements.org/page/InC/1.0/?language=en

Please cite the original version:

Hiltunen, V.-M., Koskinen, P. J., Mentel, K. K., Manninen, J., Myllyperkiö, P., Johansson, A., & Pettersson, M. (2020). Making Graphene Luminescent by Direct Laser Writing. Journal of Physical Chemistry C, 124(15), 8371-8377. https://doi.org/10.1021/acs.jpcc.0c00194

THE JOURNAL OF PHYSICAL CHEMISTRY C

Subscriber access provided by JYVASKYLAN UNIV

C: Physical Processes in Nanomaterials and Nanostructures

Making Graphene Luminescent by Direct Laser Writing

Vesa-Matti Hiltunen, Pekka Johannes Koskinen, Kamila K. Mentel, Jyrki Manninen, Pasi Myllyperkiö, Andreas Johansson, and Mika Pettersson

J. Phys. Chem. C, **Just Accepted Manuscript** • DOI: 10.1021/acs.jpcc.0c00194 • Publication Date (Web): 25 Mar 2020

Downloaded from pubs.acs.org on March 26, 2020

Just Accepted

"Just Accepted" manuscripts have been peer-reviewed and accepted for publication. They are posted online prior to technical editing, formatting for publication and author proofing. The American Chemical Society provides "Just Accepted" as a service to the research community to expedite the dissemination of scientific material as soon as possible after acceptance. "Just Accepted" manuscripts appear in full in PDF format accompanied by an HTML abstract. "Just Accepted" manuscripts have been fully peer reviewed, but should not be considered the official version of record. They are citable by the Digital Object Identifier (DOI®). "Just Accepted" is an optional service offered to authors. Therefore, the "Just Accepted" Web site may not include all articles that will be published in the journal. After a manuscript is technically edited and formatted, it will be removed from the "Just Accepted" Web site and published as an ASAP article. Note that technical editing may introduce minor changes to the manuscript text and/or graphics which could affect content, and all legal disclaimers and ethical guidelines that apply to the journal pertain. ACS cannot be held responsible for errors or consequences arising from the use of information contained in these "Just Accepted" manuscripts.

is published by the American Chemical Society. 1155 Sixteenth Street N.W., Washington, DC 20036

Published by American Chemical Society. Copyright © American Chemical Society. However, no copyright claim is made to original U.S. Government works, or works produced by employees of any Commonwealth realm Crown government in the course of their duties.

Making Graphene Luminescent by Direct Laser Writing

Vesa-Matti Hiltunen,[†] Pekka Koskinen,[†] Kamila K. Mentel,[‡] Jyrki Manninen,[†] Pasi Myllyperkiö,[‡] Andreas Johansson,[*,†,‡] and Mika Pettersson[*,‡]

†*Nanoscience center, Department of Physics, University of Jyväskylä, 40014 Jyväskylä, Finland*

‡*Nanoscience center, Department of Chemistry, University of Jyväskylä, 40014 Jyväskylä, Finland*

E-mail: andreas.johansson@jyu.fi; mika.j.pettersson@jyu.fi

Abstract

Graphene is not intrinsically luminescent, due to a lack of bandgap, and methods for its creation are tricky for device fabrication. In this study, we create luminescent graphene patterns by a simple direct laser writing method. We analyze the graphene using Raman spectroscopy and find that the laser writing leads to generation of line defects after initial formation of point defects. This Raman data enables us to create a model that explains the luminescence by a formation of small domains due to confinement of graphene by line defects, which is conceptually similar to the mechanism of luminescence in graphene quantum dots.

Introduction

Pristine graphene is not luminescent due to the absence of band gap and the rapid nonradiative relaxation of electrons and holes.[1–4] However, there are methods to obtain broad-

band luminescence from graphene. For instance, the luminescence can arise from graphene under high doping conditions[5], from graphene oxide,[6–8] and from graphene quantum dots (GQDs).[9–12] While the luminescence can be obtained by these means, their implementation to devices is not straightforward. Therefore, it would be highly beneficial to find other, more practical means to locally modify graphene to achieve luminescent properties.

Fortunately, the properties of graphene can be modified by laser irradiation.[13–17] Laser modification is simple, it omits chemicals, and it enables writing patterns. For example, femtosecond laser irradiation can be used to oxidize graphene without losing the integrity of the carbon network.[18] When irradiation is carried out under inert gas atmosphere, three-dimensional structures are formed in a process termed "optical forging".[19] The primary process responsible for optical forging is known to be the generation of defects, although the understanding of the process still remains incomplete.

In this work, we report that optically forged graphene exhibits unexpected strong photoluminescence. We study the origin of this irradiation-induced photoluminescence in graphene using Raman spectroscopy. It gives insight into the pulsed laser patterning process since it is sensitive to graphene's lattice defects,[20–24] doping levels[5,25–32] and strain,[33–36] and with careful analysis it is possible to differentiate these contributions from each other.[37–41] By combining the Raman measurements with theoretical modeling, we are able to develop a convincing model for the luminescence: it can be explained by formation of small domains due to confinement of graphene by line defects, which is conceptually similar to mechanism of luminescence of graphene quantum dots.

Experimental section

The graphene was synthesized with chemical vapor deposition (CVD) on copper thin film and transferred onto a Si/SiO_x substrate using a normal PMMA transfer method.[42] The graphene was then patterned with a tightly focused femtosecond laser in nitrogen atmosphere

by raster scanning the sample over the pulsed laser beam with a piezo stage. After the direct laser writing, the processed areas were characterized by atomic force microscope imaging and by Raman mapping. For details of the fabrication process, direct laser writing and characterizations, see Supporting Information (SI).

Results and discussion

Experimental observation of luminescence

The result of the pulsed laser patterning is shown in Figure 1a. Each square pattern in the figure has a different exposure time per spot, and the heights of the patterns increase with increasing exposure time, as reported before.[19] Raman spectra from the middle of each square are shown in Figure 1b. The irradiation dose is an experimental parameter defined by multiplying the pulse energy with irradiation time per spot. This definition helps to compare results obtained with different pulse energies and/or exposure times. There are three notable developments in these Raman spectra as irradiation dose increases. First, the 2D graphene Raman band intensity decreases, diminishing almost completely at the highest dose. Second, the D and G bands both broaden and increase in intensity. Third, there is an appearance of a wide photoluminescence signal. The intensity of the signal increases consistently with increasing irradiation dose (Figures 1b and 1c). For example, at the highest dose in Figure 1b, the integrated intensity of the photoluminescence is over 400 times stronger than the G band intensity in unpatterned graphene. We extracted photoluminescence spectra from the Raman data (Figure 1d). These spectra showcase that the emission is very broad, extending nearly the entire visible range.

There are several reports of photoluminescence arising from different graphene-based materials. One of such materials is graphene oxide.[6–8] However, we have previously determined, based on X-ray photoelectron spectroscopy, that our laser written patterns contain only carbon.[19] Chen et al. observed photoluminescence signal from graphene under high

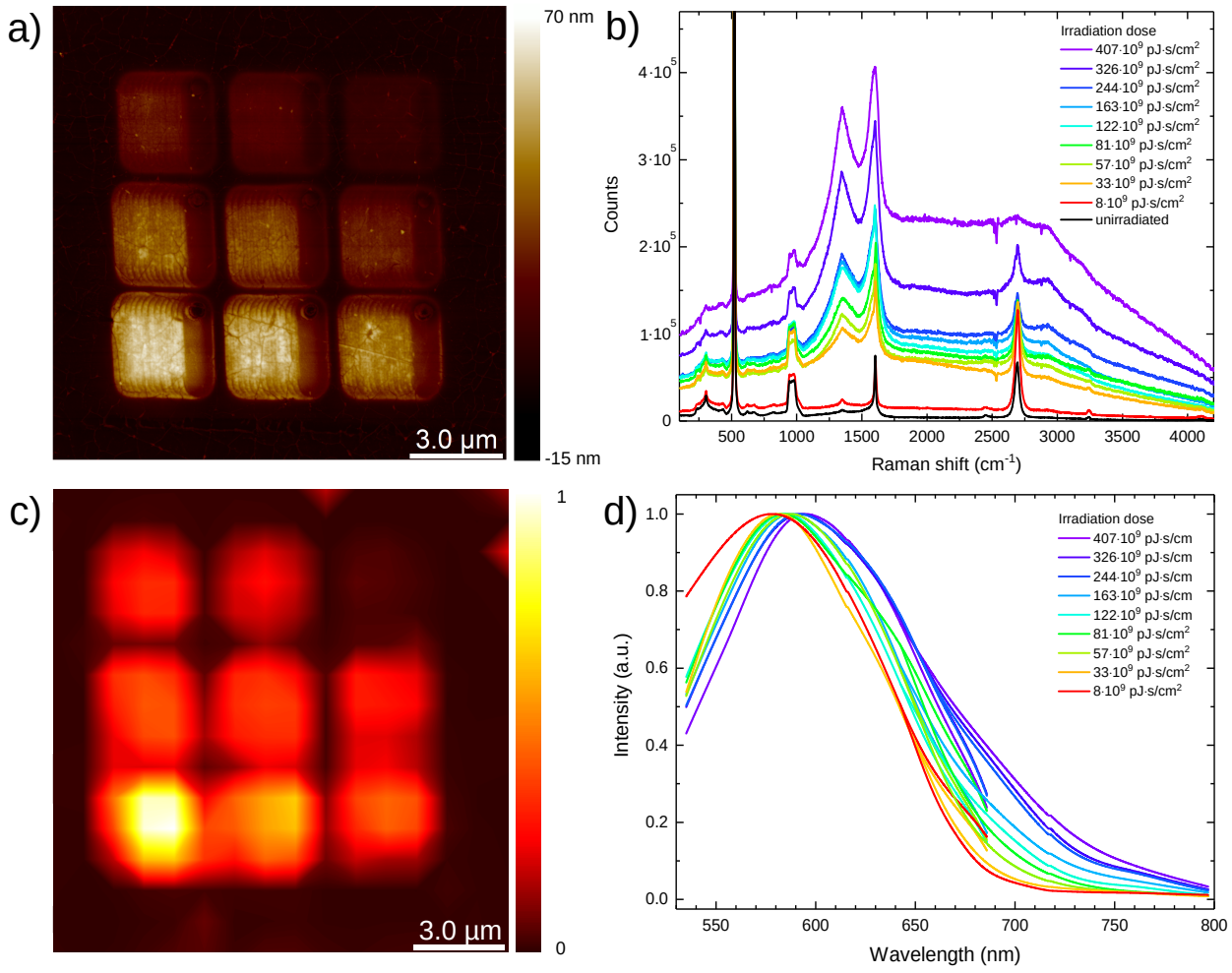

Figure 1: Characterization of the photoluminescent graphene patterns. a) An atomic force microscope image of a pattern set made with 160 pJ pulse energy. Exposure dose increases from up to down and right to left. Height of the patterns increase with the exposure dose. b) Raman spectra from the middle of each pattern measured with 532 nm excitation wavelength. c) A photoluminescence map of the same patterns as in panel a. The intensity is integrated between $1800 - 2500\ \mathrm{cm}^{-1}$ ($588 - 614$ nm). d) Normalized PL spectra extracted from the Raman spectra in panel b and Figure S1c. The spectra are baselines from asymmetric least squares smoothing process. The shorter wavelength part is extracted from Raman spectra measured with 532 nm laser excitation and the long wavelength tail from 633 nm excitation (Figure S1c).

p-type doping, which empties states in the valence band and enables a broadband emission.[5] Heller et al. assigned this photoluminescence to electronic Raman scattering.[43] We analyzed doping and strain of our samples from the shifts of G and 2D bands in Raman spectra (for details, see SI). The analysis revealed that the doping levels in our samples are too low to create emission in the visible region via this mechanism.

Photoluminescence could arise also from graphene quantum dots. The spectral characteristics of some GQDs in literature are at least qualitatively similar to the spectra in Figure 1d.[9–12] Should the cause of the photoluminescence in our samples be the formation of structures akin to quantum dots, the pulsed laser irradiation would have to form isolated graphene islands. We have determined previously that the pulsed laser irradiation does form lattice defects in graphene,[19] but here the point- and line-type character of the defects are analyzed for the first time.

From point to line defects

In order to get a more complete picture about the defect formation during the irradiation, we prepared four additional sets with pulse energies of 140 pJ, 120 pJ, 70 pJ and 30 pJ, in addition to the pattern set made with 160 pJ pulse energy. Raman spectra measured from these patterns (presented in SI) show that the above-mentioned changes in the graphene Raman bands happen with all pulse energies, as well as the increase of the broad photoluminescence. The photoluminescence intensities versus irradiation dose is presented in Figure 2a. The trend of intensity increase is similar with all the pulse energies, except with 30 pJ where the increase is more conservative. Also, the Raman peaks from these patterns show that there is a difference between lightly and heavily irradiated patterns. The intensity of the D band increases initially with low irradiation dose, forming a sharp D peak. The sharpness of the D peak with low irradiation dose suggests that the irradiation initially creates point defects.[24] As the irradiation dose increases and the broad background signal starts to develop, the D band transforms to a wider and less intensive peak compared to the G

peak. This indicates that the patterns made with higher dose have higher amount of line defects.[23,24]

To better understand the defect character, we estimated the amounts of point defects and line defects in pulsed laser patterned graphene following a model developed by Cançado et al.[24] (for details, see SI). This model is based on point and line defects having different effects on the Raman spectra. The main difference is that, in general, the point defects increase the integrated intensity ratio of the D and G bands (A_D/A_G),[44] while line defects increase the full width at half maximum of the G band (Γ_G)(Figure 2b).[23] The experimental values for A_D/A_G and Γ_G were acquired from fitting parameters and the defect densities were calculated from equations S1 and S. Details about the fitting and defect calculations are presented in SI.

Experimental data shows that the A_D/A_G ratio increases with all pulse energies, while the Γ_G increases further with higher pulse energies. Cançado's model enables calculating point defect densities and the crystallite sizes from the experimental data (Figures 2c and 2d). In unirradiated graphene, the point defect density is approximately 10^{11} cm^{-2}, as is common for CVD graphene. The point defect density increases sharply during the early stages of the irradiation to $1 - 5 \cdot 10^{12}$ cm^{-2} range and starts to decrease with higher doses. An outlier here is the 70 pJ case, where the density with low doses saturates to about $2 - 3 \cdot 10^{11}$ cm^{-2}. The reason for this behavior is not clear. However, since every data point in Figure 2 is from a different individual pattern, it is possible that there could be differences in the initial conditions of the graphene, such as defect or residue amounts, that would affect the defect formation process. For the three highest pulse energies the points with highest doses are omitted. This omission is because they fall under the black solid line in Figure 2b, which produces unphysical results (point defect density falls below zero).

Yet the most interesting analysis is the one of crystallite sizes (Figure 2d). Since CVD graphene typically has crystallites with size distribution from tens to hundreds of micrometers, the initial areas are large (Figure 2d). In fact, the crystallites are larger than the spot

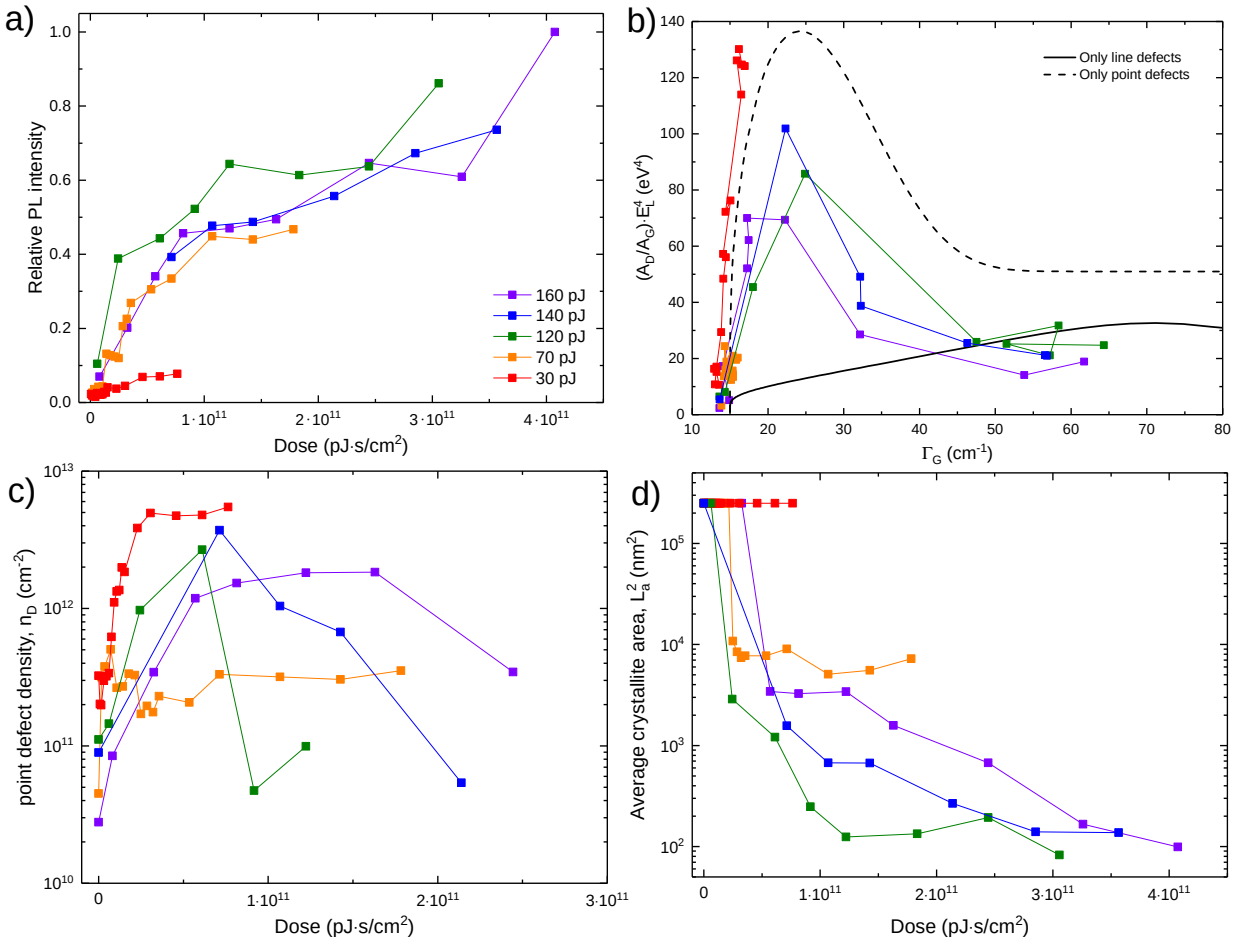

Figure 2: Defect development during pulsed laser irradiation. a) Integrated photoluminescence intensity between $1800 - 2400\ \mathrm{cm}^{-1}$ divided by integrated intensity of the G band versus pulsed irradiation dose. b) Experimental $(A_D/A_G)\,E_L^4$ as a function of Γ_G (lines with markers). The solid black line represents the case where graphene has only line defects and no point defects, and the dashed black line represents the opposite. c) Point defect density versus irradiation dose. d) Average crystallite area versus irradiation dose.

size of our Raman laser, making it impossible to estimate the crystallite sizes at low irradiation doses. The starting point of the crystallite sizes were therefore set to $2.5 \cdot 10^5$ nm^2, the estimated spot size of our Raman lasers. The crystallite size decreases sharply initially and continues to decrease with higher doses. The exception here is the 30 pJ pattern set, where the crystallite size is too large to be measurable in Raman. This pattern set is also the only one where the photoluminescence does not increase significantly during the irradiation. Interestingly, as the crystallite sizes decreases, the point defect densities saturate and even start to decrease with higher doses (Figure 2c), suggesting a gradual conversion of point defects to line defects.

Insights for defect growth from a mesoscopic model

The implications from the analysis of Raman spectra trigger several questions. What is the microscopic structure of the defects? How are point- and line defects related? What is the origin of the crystallites and their connection to luminescence?

To address these questions, we developed a model that is coherent and builds upon a plausible microscopic origin. We assume that the elementary event in the process is laser-induced creation of Stone-Wales (SW) defects, as proposed earlier.[19] The SW defect is a ninety-degree C-C bond rotation that transforms four hexagons into pairs of pentagons and heptagons (Figure S8a). The formation energy of a single SW defect in pristine graphene is around 4.6 eV, given by density-functional theory.[45] This energy coincides well with a two-photon process ($2h\nu = 4.8$ eV). While not directly indicated by our data, the notion of a two-photon process is plausible as it conforms with observations from similar experimental settings.[46] However, for our interests the most important feature in SW defects is their strong attractive and highly *anisotropic* interaction. The interaction of two SW defects depends strongly on their exact orientation and separation. In particular, defects separated precisely by two lattice constants (4.9 Å) are bound almost by 1.5 eV (SI), which implies that laser irradiation presumably prefers creating new SW defects that conform to this

favorable arrangement. This interaction motivated us to develop a kinetic defect growth model involving the formation of new SW defects (for model details, see SI).

The only parameter in the model, χ, is the ratio between the probability for forming new SW defect into any site in pristine graphene and the probability for forming new SW defects in the favorable sites. The energetics of SW interaction imply $\chi \ll 1$, but otherwise χ is a free parameter; a smaller χ implies small density of long defects, larger χ implies high density of short defects.

Using the model, the defect growth kinematics was straightforward to simulate (for details, see SI). Based on parameter values from earlier similar models[18], we used a tentative parameter $\chi = 10^{-5}$ and propagated time onward, observing point defects appearing, then growing into line defects, gradually percolating across the entire area, and ultimately filling the area with ever thickening network of line defects (Figure 3). These observations align well with the experimental results: *i*) Defects are initially point-like, but gradually turn into line defects. While existing defects keep growing, new defects keep appearing at a constant rate, resulting in rapid increase in point-defect density (Figure 2c). *ii*) Consequently, as soon as point-defect density increases sufficiently, the Raman spectra becomes governed by line defects. Moreover, once the line defects start to dominate, the area of pristine graphene starts to decrease notably, causing a reduction in the density of point defects (Figures 2c and 3c). *iii*) When line defects percolate across the entire area, they define semi-enclosed regions with electron-scattering boundaries—crystallites that can function as graphene quantum dots. *iv*) The crystallites have a broad size distribution, which implies the emission of optical wavelengths over a wide range—the luminescence of white light. In summary, the model provides reasonable explanations to all of the central experimental observations.

For quantitative comparison between the model and the experiment, we repeated the simulations with χ in the reasonable range $10^{-3} \ldots 10^{-6}$ (Figure S10). The crystallite dimensions were characterized by sampling 10^3 random confinement lengths each time step of the simulation (Figure 4a). At the percolation threshold—manifesting the instant when

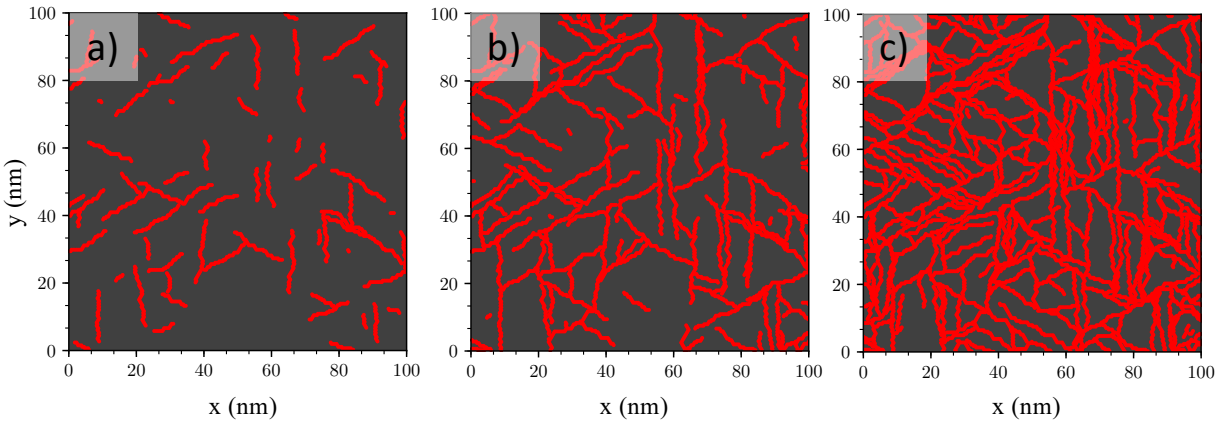

Figure 3: Appearance of line defect -defined crystallites. Panels show the temporal growth of Stone-Wales line defects with $\chi = 10^{-5}$ and a) $t = 12$, b) $t = 24$, and c) $t = 48$. The middle panel corresponds to the percolation time t_{perc}, when the line defects reach continuously across the entire irradiated area.

crystallites supposedly become sufficiently enclosed to define GQDs—the median confinement length for $\chi = 10^{-3} \ldots 10^{-6}$ ranges from 3 to 25 nm (Figure 4b). The range agrees well with the experimentally inferred crystallite size of 10 nm. The best agreement with experiment is obtained by $\chi \approx 10^{-5}$ (Figure 4b), which in retrospect motivates our tentative value for χ (Figure 3).

In addition to qualitatively explaining the Raman spectra and to quantitatively implying $\sim$ 10 nm crystallite areas, the value around $\chi \sim 10^{-5}$ is attractive for two other reasons. First, it suggests a maximum point defect density around $n_D \sim 10^{12}$ cm^{-2}, in reasonable agreement with experiments (Figure 2c). Second, a similar growth model with the same parameter value of 10^{-5} was used in a previous work to explain quantitatively the laser-induced growth of oxidized islands on graphene.[18] This conformity makes a curious connection between optical forging and laser-induced oxidation, hinting towards a similar microscopic origin in the creation of SW defects.

Crystallite area affects strongly on the luminescence, if the patterned graphene is considered analogously to the GQDs. This is because the GQD size defines its bandgap due to quantum confinement effect (QCE) of conjugated π-domains.[47–49] In literature, the GQDs

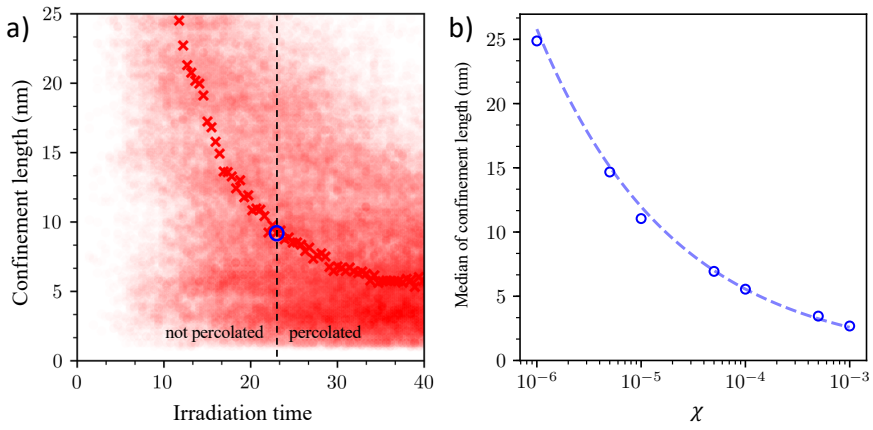

Figure 4: Quantitative analysis of confinement. a) Sampled 10^3 confinement lengths for each irradiation time ($\chi = 10^{-5}$). The cross is the median over the sampled lengths for given irradiation time, the vertical dashed line highlights the percolation threshold, and the blue sphere emphasizes the median length upon percolation. b) The confinement median lengths upon percolation for $\chi = 10^{-6} \ldots 10^{-3}$. The dashed line is an analytical estimate from Eq. (S3).

with similar spectra are in the size range of $1 - 2$ nm, while our smallest crystallite size was 10 nm. Yet it is worth noting that our value is an average value within the spot size of our Raman laser and, based on the modelling, the crystallites within this area have a quite wide size distribution. However, the mechanism of luminescence of GQDs is still under debate and the spectral properties of the GQDs are not explained by the QCE alone.[49] For example, related to the other PL mechanisms, the spectra of GQDs can change depending on chemical environment,[50–52] functional groups[53] and defects in the dots.[54,55] We currently lack direct atomic scale information about the graphene in patterned areas, which would reveal important details that affect the luminescence.

The peak positions of luminescence (Figure 1d) shift to longer wavelengths with higher dose. At first this might seem contradictory, since during irradiation the crystallite size decreases and smaller GQDs have larger bandgap. However, this can be explained just with the shifting of the size distribution: if the peak of the distribution shifts toward small crystallite area, the amount of larger (≥ 2 nm) crystallites will increase more than the smaller (≤ 2 nm) crystallites if the peak of the distribution is higher than 2 nm. This is certainly

the case in our sample, since the smallest average crystallite size measured was about 10 nm.

Conclusions

To summarize, we demonstrate a method to create photoluminescent patterns from graphene using femtosecond pulsed laser irradiation. Raman analysis revealed that the pulsed laser irradiation generates line defects in addition to point defects. To explain the luminescence, we present a model, in which the generation of the line defects confines small graphene islands that behave similarly to graphene quantum dots. The broad white light luminescence from graphene is highly interesting for applications, such as displays. Our process provides an attractive method for achieving luminescence properties from graphene, since it is local and does not require lithography or chemical treatments.

Acknowledgement

V.-M.H. acknowledges funding from the Finnish Cultural Foundation. P.K. and M.P. acknowledge funding from the Academy of Finland (grants 297115 and 311330).

Supporting Information Available

Experimental details, Raman spectra and AFM images of all pattern sets, description of Raman analyses, model for defect growth.

References

(1) Park, C.-H.; Giustino, F.; Cohen, M. L.; Louie, S. G. Velocity Renormalization and Carrier Lifetime in Graphene from the Electron-Phonon Interaction. *Phys. Rev. Lett.* **2007**, *99*, 086804.

(2) Dawlaty, J. M.; Shivaraman, S.; Chandrashekhar, M.; Rana, F.; Spencer, M. G. Measurement of Ultrafast Carrier Dynamics in Epitaxial Graphene. *Appl. Phys. Lett.* **2008**, *92*, 042116.

(3) Sun, D.; Wu, Z.-K.; Divin, C.; Li, X.; Berger, C.; de Heer, W. A.; First, P. N.; Norris, T. B. Ultrafast Relaxation of Excited Dirac Fermions in Epitaxial Graphene Using Optical Differential Transmission Spectroscopy. *Phys. Rev. Lett.* **2008**, *101*, 157402.

(4) Mak, K. F.; Ju, L.; Wang, F.; Heinz, T. F. Optical Spectroscopy of Graphene: From the Far Infrared to the Ultraviolet. *Solid State Comm.* **2012**, *152*, 1341–1349.

(5) Chen, C.-F.; Park, C.-H.; Boudouris, B. W.; Horng, J.; Geng, B.; Girit, C.; Zettl, A.; Crommie, M. F.; Segalman, R. A.; Louie, S. G.; et al., Controlling Inelastic Light Scattering Quantum Pathways in Graphene. *Nature* **2011**, *471*, 617–620.

(6) Gokus, T.; Nair, R. R.; Bonetti, A.; Böhmler, M.; Lombardo, A.; Novoselov, K. S.; Geim, A. K.; Ferrari, A. C.; Hartschuh, A. Making Graphene Luminescent by Oxygen Plasma Treatment. *ACS Nano* **2009**, *3*, 3963–3968.

(7) Peng, J.; Gao, W.; Gupta, B. K.; Liu, Z.; Romero-Aburto, R.; Ge, L.; Song, L.; Alemany, L. B.; Zhan, X.; Gao, G.; et al., Graphene Quantum Dots Derived from Carbon Fibers. *Nano Lett.* **2012**, *12*, 844–849.

(8) Shang, J.; Ma, L.; Li, J.; Ai, W.; Yu, T.; Gurzadyan, G. G. The Origin of Fluorescence from Graphene Oxide. *Sci. Rep.* **2012**, *2*, 792.

(9) Xu, Q.; Zhou, Q.; Hua, Z.; Xue, Q.; Zhang, C.; Wang, X.; Pan, D.; Xiao, M. Single-Particle Spectroscopic Measurements of Fluorescent Graphene Quantum Dots. *ACS Nano* **2013**, *7*, 10654–10661.

(10) Jiang, F.; Chen, D.; Li, R.; Wang, Y.; Zhang, G.; Li, S.; Zheng, J.; Huang, N.; Gu, Y.; Wang, C.; et al., Eco-Friendly Synthesis of Size-Controllable Amine-Functionalized

Graphene Quantum Dots with Antimycoplasma Properties. *Nanoscale* **2013**, *5*, 1137–1142.

(11) Yang, P.; Zhou, L.; Zhang, S.; Wan, N.; Pan, W.; Shen, W. Facile Synthesis and Photoluminescence Mechanism of Graphene Quantum Dots. *J. Appl. Phys.* **2014**, *116*, 244306.

(12) Li, L.; Wu, G.; Yang, G.; Peng, J.; Zhao, J.; Zhu, J.-J. Focusing on Luminescent Graphene Quantum Dots: Current Status and Future Perspectives. *Nanoscale* **2013**, *5*, 4015–4039.

(13) Yoo, J.-H.; Kim, E.; Hwang, D. J. Femtosecond Laser Patterning, Synthesis, Defect Formation, and Structural Modification of Atomic Layered Materials. *MRS Bull.* **2016**, *41*, 1002–1008.

(14) Stöhr, R. J.; Kolesov, R.; Xia, K.; Wrachtrup, J. All-Optical High-Resolution Nanopatterning and 3D Suspending of Graphene. *ACS Nano* **2011**, *5*, 5141–5150.

(15) Zhang, W.; Li, L.; Wang, Z. B.; Pena, A. A.; Whitehead, D. J.; Zhong, M. L.; Lin, Z.; Zhu, H. W. Ti:Sapphire Femtosecond Laser Direct Micro-Cutting and Profiling of Graphene. *Appl. Phys. A* **2012**, *109*, 291–297.

(16) Kiisk, V.; Kahro, T.; Kozlova, J.; Matisen, L.; Alles, H. Nanosecond Laser Treatment of Graphene. *Appl. Surf. Sci.* **2013**, *276*, 133–137.

(17) Yoo, J.-H.; Park, J. B.; Ahn, S.; Grigoropoulos, C. P. Laser-Induced Direct Graphene Patterning and Simultaneous Transferring Method for Graphene Sensor Platform. *Small* **2013**, *9*, 4269–4275.

(18) Aumanen, J.; Johansson, A.; Koivistoinen, J.; Myllyperkiö, P.; Pettersson, M. Patterning and Tuning of Electrical and Optical Properties of Graphene by Laser Induced Two-Photon Oxidation. *Nanoscale* **2015**, *7*, 2851–2855.

(19) Johansson, A.; Myllyperkiö, P.; Koskinen, P.; Aumanen, J.; Koivistoinen, J.; Tsai, H.-C.; Chen, C.-H.; Chang, L.-Y.; Hiltunen, V.-M.; Manninen, J. J.; et al., Optical Forging of Graphene into Three-Dimensional Shapes. *Nano Lett.* **2017**, *17*, 6469–6474.

(20) Pimenta, M. A.; Dresselhaus, G.; Dresselhaus, M. S.; Cançado, L. G.; Jorio, A.; Saito, R. Studying Disorder in Graphite-Based Systems by Raman Spectroscopy. *Phys. Chem. Chem. Phys.* **2007**, *9*, 1276–1290.

(21) Cançado, L. G.; Takai, K.; Enoki, T.; Endo, M.; Kim, Y. A.; Mizusaki, H.; Jorio, A.; Coelho, L. N.; Magalhães-Paniago, R.; Pimenta, M. A. General Equation for the Determination of the Crystallite Size La of Nanographite by Raman Spectroscopy. *Appl. Phys. Lett.* **2006**, *88*, 163106.

(22) Lucchese, M.; Stavale, F.; Ferreira, E. M.; Vilani, C.; Moutinho, M.; Capaz, R. B.; Achete, C.; Jorio, A. Quantifying Ion-Induced Defects and Raman Relaxation Length in Graphene. *Carbon* **2010**, *48*, 1592–1597.

(23) Ribeiro-Soares, J.; Oliveros, M.; Garin, C.; David, M.; Martins, L.; Almeida, C.; Martins-Ferreira, E.; Takai, K.; Enoki, T.; Magalhães-Paniago, R.; et al., Structural Analysis of Polycrystalline Graphene Systems by Raman Spectroscopy. *Carbon* **2015**, *95*, 646–652.

(24) Cançado, L. G.; da Silva, M. G.; Ferreira, E. H. M.; Hof, F.; Kampioti, K.; Huang, K.; Pénicaud, A.; Achete, C. A.; Capaz, R. B.; Jorio, A. Disentangling Contributions of Point and Line Defects in the Raman Spectra of Graphene-Related Materials. *2D Mater.* **2017**, *4*, 025039.

(25) Casiraghi, C.; Pisana, S.; Novoselov, K. S.; Geim, A. K.; Ferrari, A. C. Raman Fingerprint of Charged Impurities in Graphene. *Appl. Phys. Lett.* **2007**, *91*, 233108.

(26) Yan, J.; Zhang, Y.; Kim, P.; Pinczuk, A. Electric Field Effect Tuning of Electron-Phonon Coupling in Graphene. *Phys. Rev. Lett.* **2007**, *98*, 166802.

(27) Das, A.; Chakraborty, B.; Piscanec, S.; Pisana, S.; Sood, A. K.; Ferrari, A. C. Phonon Renormalization in Doped Bilayer Graphene. *Phys. Rev. B* **2009**, *79*, 155417.

(28) Pisana, S.; Lazzeri, M.; Casiraghi, C.; Novoselov, K. S.; Geim, A. K.; Ferrari, A. C.; Mauri, F. Breakdown of the Adiabatic Born-Oppenheimer Approximation in Graphene. *Nat. Mater.* **2007**, *6*, 198–201.

(29) Das, A.; Pisana, S.; Chakraborty, B.; Piscanec, S.; K Saha, S.; Waghmare, U.; S Novoselov, K.; Krishnamurthy, H.; Geim, A.; Ferrari, A.; et al., Monitoring Dopants by Raman Scattering in an Electrochemically Top-Gated Graphene Transistor. *Nat. Nanotechnol.* **2008**, *3*, 210–215.

(30) Basko, D. M.; Piscanec, S.; Ferrari, A. C. Electron-Electron Interactions and Doping Dependence of the Two-Phonon Raman Intensity in Graphene. *Phys. Rev. B* **2009**, *80*, 165413.

(31) Kalbáč, M.; Reina-Cecco, A.; Farhat, H.; Kong, J.; Kavan, L.; Dresselhaus, M. S. The Influence of Strong Electron and Hole Doping on the Raman Intensity of Chemical Vapor-Deposition Graphene. *ACS Nano* **2010**, *4*, 6055–6063.

(32) Casiraghi, C. Probing Disorder and Charged Impurities in Graphene by Raman Spectroscopy. *Phys. Status Solidi RRL* **2009**, *3*, 175–177.

(33) Ding, F.; Ji, H.; Chen, Y.; Herklotz, A.; Dörr, K.; Mei, Y.; Rastelli, A.; Schmidt, O. G. Stretchable Graphene: A Close Look at Fundamental Parameters through Biaxial Straining. *Nano Lett.* **2010**, *10*, 3453–3458.

(34) Androulidakis, C.; Tsoukleri, G.; Koutroumanis, N.; Gkikas, G.; Pappas, P.; Parthenios, J.; Papagelis, K.; Galiotis, C. Experimentally Derived Axial Stress-Strain Relations for Two-Dimensional Materials Such as Monolayer Graphene. *Carbon* **2015**, *81*, 322–328.

(35) Tsoukleri, G.; Parthenios, J.; Papagelis, K.; Jalil, R.; Ferrari, A. C.; Geim, A. K.; Novoselov, K. S.; Galiotis, C. Subjecting a Graphene Monolayer to Tension and Compression. *Small* **2009**, *5*, 2397–2402.

(36) Zabel, J.; Nair, R. R.; Ott, A.; Georgiou, T.; Geim, A. K.; Novoselov, K. S.; Casiraghi, C. Raman Spectroscopy of Graphene and Bilayer under Biaxial Strain: Bubbles and Balloons. *Nano Lett.* **2012**, *12*, 617–621.

(37) Liu, J.; Li, Q.; Zou, Y.; Qian, Q.; Jin, Y.; Li, G.; Jiang, K.; Fan, S. The Dependence of Graphene Raman D-band on Carrier Density. *Nano Lett.* **2013**, *13*, 6170–6175.

(38) Beams, R.; Cançado, L. G.; Novotny, L. Raman Characterization of Defects and Dopants in Graphene. *J. Phys.: Condens. Matter* **2015**, *27*, 083002.

(39) Mueller, N. S.; Heeg, S.; Alvarez, M. P.; Kusch, P.; Wasserroth, S.; Clark, N.; Schedin, F.; Parthenios, J.; Papagelis, K.; Galiotis, C.; et al., Evaluating Arbitrary Strain Configurations and Doping in Graphene with Raman Spectroscopy. *2D Mater.* **2017**, *5*, 015016.

(40) Bruna, M.; Ott, A. K.; Ijäs, M.; Yoon, D.; Sassi, U.; Ferrari, A. C. Doping Dependence of the Raman Spectrum of Defected Graphene. *ACS Nano* **2014**, *8*, 7432–7441.

(41) Lee, J. E.; Ahn, G.; Shim, J.; Lee, Y. S.; Ryu, S. Optical Separation of Mechanical Strain from Charge Doping in Graphene. *Nat. Commun.* **2012**, *3*, 1024.

(42) Suk, J. W.; Kitt, A.; Magnuson, C. W.; Hao, Y.; Ahmed, S.; An, J.; Swan, A. K.; Goldberg, B. B.; Ruoff, R. S. Transfer of CVD-Grown Monolayer Graphene onto Arbitrary Substrates. *ACS Nano* **2011**, *5*, 6916–6924.

(43) Heller, E. J.; Yang, Y.; Kocia, L.; Chen, W.; Fang, S.; Borunda, M.; Kaxiras, E. Theory of Graphene Raman Scattering. *ACS Nano* **2016**, *10*, 2803–2818.

(44) Martins Ferreira, E. H.; Moutinho, M. V. O.; Stavale, F.; Lucchese, M. M.; Capaz, R. B.; Achete, C. A.; Jorio, A. Evolution of the Raman Spectra from Single-, Few-, and Many-Layer Graphene with Increasing Disorder. *Phys. Rev. B* **2010**, *82*, 125429.

(45) Ma, J.; Alfè, D.; Michaelides, A.; Wang, E. Stone-Wales Defects in Graphene and Other Planar sp2 -Bonded Materials. *Phys. Rev. B* **2009**, *80*, 033407.

(46) Koivistoinen, J.; Sladkova, L.; Aumanen, J.; Koskinen, P. J.; Roberts, K.; Johansson, A.; Myllyperkiö, P.; Pettersson, M. From Seeds to Islands: Growth of Oxidized Graphene by Two-Photon Oxidation. *J. Phys. Chem. C* **2016**, *120*, 22330.

(47) Song, Y.; Zhao, X.; Shao, J.; Zhang, J.; Yang, B. The Photoluminescence Mechanism in Carbon Dots (Graphene Quantum Dots, Carbon Nanodots, and Polymer Dots): Current State and Future Perspective. *Nano Res.* **2015**, *8*, 355–381.

(48) Carbonaro, C. M.; Corpino, R.; Salis, M.; Mocci, F.; Thakkar, S. V.; Olla, C.; Ricci, P. C. On the Emission Properties of Carbon Dots: Reviewing Data and Discussing Models. *C* **2019**, *5*, 60.

(49) Zhu, S.; Song, Y.; Wang, J.; Wan, H.; Zhang, Y.; Ning, Y.; Yang, B. Photoluminescence Mechanism in Graphene Quantum Dots: Quantum Confinement Effect and Surface/Edge State. *Nano Today* **2017**, *13*, 10–14.

(50) Zhu, S.; Zhang, J.; Qiao, C.; Tang, S.; Li, Y.; Yuan, W.; Li, B.; Tian, L.; Liu, F.; Hu, R.; et al., Strongly Green-Photoluminescent Graphene Quantum Dots for Bioimaging Applications. *Chem. Commun.* **2011**, *47*, 6858–6860.

(51) Tachi, S.; Morita, H.; Takahashi, M.; Okabayashi, Y.; Hosokai, T.; Sugai, T.; Kuwahara, S. Quantum Yield Enhancement in Graphene Quantum Dots via Esterification with Benzyl Alcohol. *Sci. Rep.* **2019**, *9*, 14115.

(52) Tetsuka, H.; Asahi, R.; Nagoya, A.; Okamoto, K.; Tajima, I.; Ohta, R.; Okamoto, A. Optically Tunable Amino-Functionalized Graphene Quantum Dots. *Adv. Mater.* **2012**, *24*, 5333–5338.

(53) Qu, D.; Zheng, M.; Li, J.; Xie, Z.; Sun, Z. Tailoring Color Emissions From N-Doped Graphene Quantum Dots for Bioimaging Applications. *Light: Sci. Appl.* **2015**, *4*, e364.

(54) Zhu, S.; Zhang, J.; Liu, X.; Li, B.; Wang, X.; Tang, S.; Meng, Q.; Li, Y.; Shi, C.; Hu, R.; et al., Graphene Quantum Dots with Controllable Surface Oxidation, Tunable Fluorescence and Up-Conversion Emission. *RSC Adv.* **2012**, *2*, 2717–2720.

(55) Pan, D.; Zhang, J.; Li, Z.; Wu, M. Hydrothermal Route for Cutting Graphene Sheets into Blue-Luminescent Graphene Quantum Dots. *Adv. Mater.* **2010**, *22*, 734–738.

Graphical TOC Entry